Theoretical study of fcc-metal/MgO(110) interfacial potentials

2010 J. Phys.: Condens. Matter 22 215001

(http://iopscience.iop.org/0953-8984/22/21/215001)

J. Phys.: Condens. Matter **22** (2010) 215001 (11pp) doi:10.1088/0953-8984/22/21/215001

Theoretical study of fcc-metal/MgO(110) interfacial potentials

Jie Chen[1] **and Nanxian Chen**[1,2]

[1] Department of Physics, Tsinghua University, Beijing 100084, People's Republic of China
[2] Institute for Applied Physics, University of Science and Technology, Beijing 10084, People's Republic of China

E-mail: chenjie-01@tsinghua.org.cn

Received 31 December 2009, in final form 25 March 2010
Published 30 April 2010
Online at stacks.iop.org/JPhysCM/22/215001

Abstract

Most studies on metal/MgO interfaces have focused on the metal/MgO(001) and metal/MgO(111) interfaces, but few studies have discussed the metal/MgO(110) interface. In this work, an appropriate inversion formula is deduced specifically for fcc-metal/MgO(110) (metal = Al, Ni, Pd, Cu, Ag, Au) interfaces. The required interatomic potentials across the interface are extracted from *ab initio* adhesive energy calculations by using a generalized Möbius inversion method. The differences between the metal/MgO(110) and metal/MgO(001) systems are discussed in detail. In addition, we use all relevant potentials to investigate the fracture processes for both Pd(001)/MgO(001) and Pd(110)/MgO(110) interfaces including the oxygen vacancies. The results suggest that the fractures occur between the first and second monolayer of the Pd slab for Pd(110)/MgO(110) and right at the interface for Pd(001)/MgO(001).

(Some figures in this article are in colour only in the electronic version)

1. Introduction

The metal–ceramic interface is an important issue in catalysis, transistors, anticorrosion coatings, etc [1–3]. Its unique atomic and electronic structures usually lead to particular chemical and physical properties, thus attracting many theoretical and experimental studies [4–8].

In this work, we are interested in metal/MgO interfaces, which are one of the most widely studied topics. Actually, a large number of *ab initio* calculations have been performed on this system, focusing on the electronic properties and ideal interface structures. However, the *ab initio* method is very costly for large-scale simulations, which are usually necessary for some interface problems such as misfit dislocations and wetting. So an atomistic simulation based on interatomic potentials is required.

In fact, empirical potentials across interfaces are a long-studied problem, and have not been solved until now. For metal/MgO(001) interfaces, Finnis and Duffy *et al* [9, 10] developed a discrete classical model (DCM) in the 1990s, but this model is not very widely used due to some limitations. In 2005, we found a way to derive the interfacial potentials from *ab initio* adhesive energies analytically, called the Chen–Möbius inversion method [11]. In the past few years, we have used it to study many interfaces including metal/MgO(001) ones [12–14]. It is very important that the potentials are strongly associated with the interface orientation. So for metal/MgO(001) and metal/MgO(110) interfaces, their potentials may be different, corresponding to the quite different electronic structures on the interfaces. This is the purpose of the present work, to obtain the interatomic potentials for metal/MgO(110) interfaces, and find their applications.

The paper is organized as follows. In section 2, an inversion formula for fcc-M/MgO(110) (M = Al, Ni, Pd, Cu, Ag, Au) interfaces is derived, in which a series of interfacial potentials are extracted from *ab initio* adhesive energy calculations. In section 3, a fracture on Pd/MgO(110) is investigated and the result is compared with that on Pd/MgO(001), where the vacancies on the MgO surface are taken into account. Finally, section 4 is the conclusion.

2. Methodology

2.1. Interface structure

Before deriving the interfacial potentials, we would like to give a brief description of the metal/MgO(110) interface. Virtual structures with two interfaces are adopted in this work, as

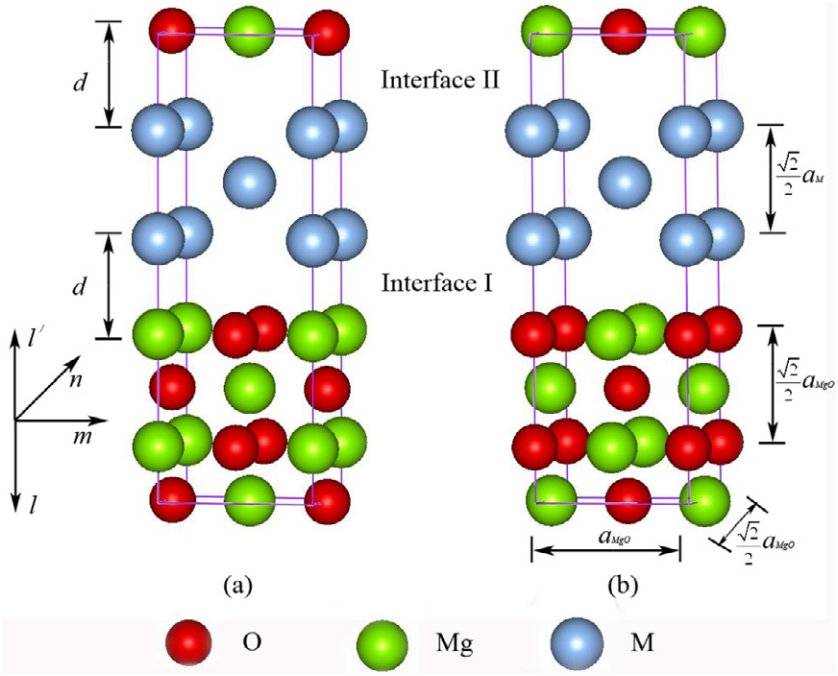

Figure 1. Two-interface structures of M/MgO(110): (a) metal on top of Mg ion, (b) metal on top of O ion. In this figure, d is the interfacial distance, a_{M} and a_{MgO} are the lattice constants of metal and MgO, respectively.

Table 1. DFT calculations of the lattice constants of MgO (a_{MgO}) and metals (a_{M}, M = Al, Ni, Pd, Cu, Ag, Au), and the corresponding interfacial misfits (defined by $2(a_{\mathrm{MgO}} - a_{\mathrm{M}})/(a_{\mathrm{MgO}} + a_{\mathrm{M}})$).

	MgO	Al	Ni	Pd	Cu	Ag	Au
Lattice constants (Å)	4.17	3.99	3.42	3.85	3.52	4.02	4.06
Misfit (%)		4.41	19.76	7.98	16.9	3.66	2.67

illustrated in figure 1. These structures are chosen carefully to help simplify the inversion of potentials. Table 1 shows their lattice constants and interfacial misfits. The former are calculated by the Vienna *Ab Initio* Simulation Package (VASP) and the latter are used to evaluate the matchable extent of a certain interface. For convenience, we force the lattices of bulk metals to match that of bulk MgO at the interface.

We adopt the pair potential approach to study the metal/MgO interfaces, just like in our previous studies [12–14]. According to the definition of the interfacial adhesive energy (E_{ad}), it can be obtained by subtracting the contributions of metal and MgO parts from the total energy. Therefore, E_{ad} is equal to the summation over all pair interactions across the interfaces and can be written as:

$$E_{\mathrm{ad}} = E_{\mathrm{total}} - E_{\mathrm{MgO}} - E_{\mathrm{M}} = \sum_{i,j} \Phi_{\mathrm{M-Mg}}(r_{ij}) + \sum_{i',j'} \Phi_{\mathrm{M-O}}(r_{i'j'}) \quad (1)$$

where E_{total} is the total energy, E_{MgO} and E_{M} are the partial energies of MgO and metal slabs, i, j, i', j' are the atomic identifications across the interfaces, r_{ij} and $r_{i'j'}$ are the pair distances. Usually, E_{ad} can be obtained by *ab initio* calculations. Our purpose is to get $\Phi_{\mathrm{M-Mg}}$ and $\Phi_{\mathrm{M-O}}$ from E_{ad}s data by solving equation (1).

2.2. Details of ab initio calculations

In this work, all *ab initio* calculations are implemented in VASP [15], based on density functional theory (DFT) with the projector augmented wave-generalized gradient approximation (PAW-GGA) method [16, 17]. These calculations are used to obtain the lattice constants in table 1 and the interfacial adhesive energy demonstrated in figure 2.

The plane-wave cutoff energy is 450 eV for the calculations of lattice constants, with a k-mesh of $7 \times 7 \times 7$. As for the calculation of the interfacial adhesive energy, the plane-wave cutoff energy is expanded up to 500 eV, with a k-mesh of $5 \times 5 \times 1$. In addition, it should be noted that the model displayed in figure 1 is just used to make it easier for readers to know how to get equation (1). Actually, we use a model consisting of four layers of MgO and five layers of metal to calculate the interfacial adhesive energy. The adhesive energy changes little with more layers of MgO or metal.

2.3. Inversion formula

Now, the Pd/MgO(110) interface is used as an example to present the main derivation. The two models in figures 1(a) and (b) are just Mg and O ions exchanged. So the difference between their adhesive energy expressions (denoted as $E_{\mathrm{Pd\to Mg}}$ and $E_{\mathrm{Pd\to O}}$, respectively) is just the exchange of $\Phi_{\mathrm{Pd-Mg}}$ and $\Phi_{\mathrm{Pd-O}}$. According to the interface structures in figure 1, the formula for $E_{\mathrm{Pd\to Mg}}$ is

$$E_{\mathrm{Pd\to Mg}}(d) = \sum_{l,l'=0}^{\infty} \sum_{m,n=-\infty}^{\infty} \left\{ \Phi_{\mathrm{Pd-Mg}} \left(\left[\left(d + l\left(\frac{\sqrt{2}}{2} a_{\mathrm{MgO}}\right) + l'\left(\frac{\sqrt{2}}{2} a_{\mathrm{Pd}}\right)\right)^2 + \left(\sqrt{2} m \left(\frac{\sqrt{2}}{2} a_{\mathrm{MgO}}\right)\right)^2 \right.\right.$$

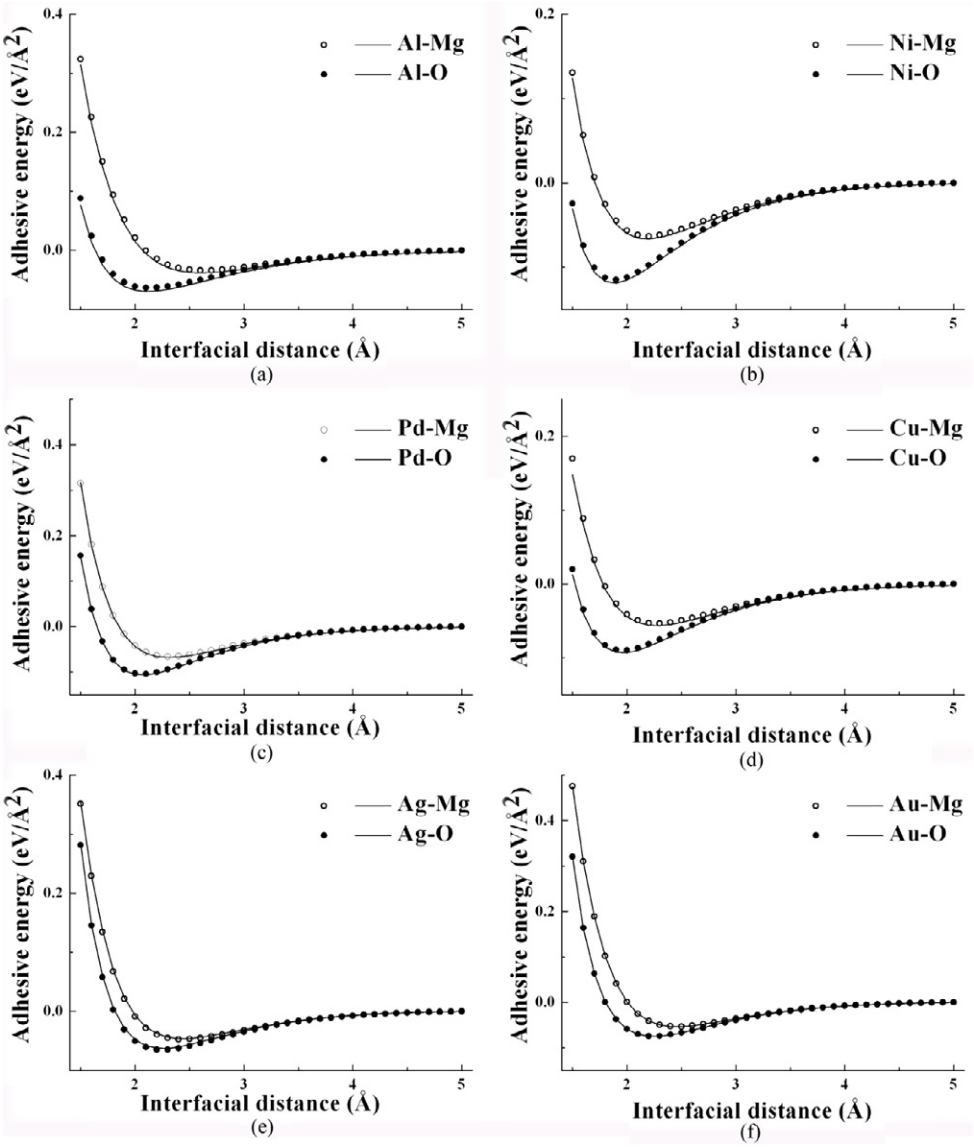

Figure 2. Adhesive energy versus d curves of M/MgO(110) interfaces. Circles are original *ab initio* data, and solid curves are recalculated data by interfacial potentials.

$$+\left(n\left(\frac{\sqrt{2}}{2}a_{\mathrm{MgO}}\right)\right)^2\Bigg]^{1/2}\Bigg)$$
$$+\Phi_{\mathrm{Pd-Mg}}\Bigg(\Bigg[\left(d+(l+1/2)\left(\frac{\sqrt{2}}{2}a_{\mathrm{MgO}}\right)\right.$$
$$\left.+l'\left(\frac{\sqrt{2}}{2}a_{\mathrm{Pd}}\right)\right)^2+\left(\sqrt{2}(m+1/2)\left(\frac{\sqrt{2}}{2}a_{\mathrm{MgO}}\right)\right)^2$$
$$+\left((n+1/2)\left(\frac{\sqrt{2}}{2}a_{\mathrm{MgO}}\right)\right)^2\Bigg]^{1/2}\Bigg)$$
$$+\Phi_{\mathrm{Pd-Mg}}\Bigg(\Bigg[\left(d+l\left(\frac{\sqrt{2}}{2}a_{\mathrm{MgO}}\right)\right.$$
$$\left.+(l'+1/2)\left(\frac{\sqrt{2}}{2}a_{\mathrm{Pd}}\right)\right)^2$$
$$+\left(\sqrt{2}(m+1/2)\left(\frac{\sqrt{2}}{2}a_{\mathrm{MgO}}\right)\right)^2$$

$$+\left((n+1/2)\left(\frac{\sqrt{2}}{2}a_{\mathrm{MgO}}\right)\right)^2\Bigg]^{1/2}\Bigg)$$
$$+\Phi_{\mathrm{Pd-Mg}}\Bigg(\Bigg[\left(d+(l+1/2)\left(\frac{\sqrt{2}}{2}a_{\mathrm{MgO}}\right)\right.$$
$$\left.+(l'+1/2)\left(\frac{\sqrt{2}}{2}a_{\mathrm{Pd}}\right)\right)^2+\left(\sqrt{2}m\left(\frac{\sqrt{2}}{2}a_{\mathrm{MgO}}\right)\right)^2$$
$$+\left(n\left(\frac{\sqrt{2}}{2}a_{\mathrm{MgO}}\right)\right)^2\Bigg]^{1/2}\Bigg)$$
$$+\Phi_{\mathrm{Pd-Mg}}\Bigg(\Bigg[\left(d+l\left(\frac{\sqrt{2}}{2}a_{\mathrm{MgO}}\right)\right.$$
$$\left.+l'\left(\frac{\sqrt{2}}{2}a_{\mathrm{Pd}}\right)\right)^2+\left(\sqrt{2}(m+1/2)\left(\frac{\sqrt{2}}{2}a_{\mathrm{MgO}}\right)\right)^2$$
$$+\left((n+1/2)\left(\frac{\sqrt{2}}{2}a_{\mathrm{MgO}}\right)\right)^2\Bigg]^{1/2}\Bigg)$$

$$
\begin{aligned}
&+\Phi_{\mathrm{Pd-Mg}}\Bigg(\Bigg[\Bigg(d+(l+1/2)\Big(\frac{\sqrt{2}}{2}a_{\mathrm{MgO}}\Big)\Big)^2+\Big(l'\Big(\frac{\sqrt{2}}{2}a_{\mathrm{Pd}}\Big)\Big)^2+\Big(\sqrt{2}m\Big(\frac{\sqrt{2}}{2}a_{\mathrm{MgO}}\Big)\Big)^2\\
&+\Big(n\Big(\frac{\sqrt{2}}{2}a_{\mathrm{MgO}}\Big)\Big)^2\Bigg]^{1/2}\Bigg)\\
&+\Phi_{\mathrm{Pd-Mg}}\Bigg(\Bigg[\Bigg(d+l\Big(\frac{\sqrt{2}}{2}a_{\mathrm{MgO}}\Big)\Big)^2+\Big((l'+1/2)\Big(\frac{\sqrt{2}}{2}a_{\mathrm{Pd}}\Big)\Big)^2+\Big(\sqrt{2}m\Big(\frac{\sqrt{2}}{2}a_{\mathrm{MgO}}\Big)\Big)^2\\
&+\Big(n\Big(\frac{\sqrt{2}}{2}a_{\mathrm{MgO}}\Big)\Big)^2\Bigg]^{1/2}\Bigg)\\
&+\Phi_{\mathrm{Pd-Mg}}\Bigg(\Bigg[\Bigg(d+(l+1/2)\Big(\frac{\sqrt{2}}{2}a_{\mathrm{MgO}}\Big)\Big)^2+\Big((l'+1/2)\Big(\frac{\sqrt{2}}{2}a_{\mathrm{Pd}}\Big)\Big)^2+\Big(\sqrt{2}(m+1/2)\\
&\times\Big(\frac{\sqrt{2}}{2}a_{\mathrm{MgO}}\Big)\Big)^2+\Big((n+1/2)\Big(\frac{\sqrt{2}}{2}a_{\mathrm{MgO}}\Big)\Big)^2\Bigg]^{1/2}\Bigg)\\
&+\Phi_{\mathrm{Pd-O}}\Bigg(\Bigg[\Bigg(d+l\Big(\frac{\sqrt{2}}{2}a_{\mathrm{MgO}}\Big)\Big)^2+\Big(l'\Big(\frac{\sqrt{2}}{2}a_{\mathrm{Pd}}\Big)\Big)^2+\Big(\sqrt{2}(m+1/2)\Big(\frac{\sqrt{2}}{2}a_{\mathrm{MgO}}\Big)\Big)^2\\
&+\Big(n\Big(\frac{\sqrt{2}}{2}a_{\mathrm{MgO}}\Big)\Big)^2\Bigg]^{1/2}\Bigg)\\
&+\Phi_{\mathrm{Pd-O}}\Bigg(\Bigg[\Bigg(d+(l+1/2)\Big(\frac{\sqrt{2}}{2}a_{\mathrm{MgO}}\Big)\Big)^2+\Big(l'\Big(\frac{\sqrt{2}}{2}a_{\mathrm{Pd}}\Big)\Big)^2+\Big(\sqrt{2}m\Big(\frac{\sqrt{2}}{2}a_{\mathrm{MgO}}\Big)\Big)^2\\
&+\Big((n+1/2)\Big(\frac{\sqrt{2}}{2}a_{\mathrm{MgO}}\Big)\Big)^2\Bigg]^{1/2}\Bigg)\\
&+\Phi_{\mathrm{Pd-O}}\Bigg(\Bigg[\Bigg(d+l\Big(\frac{\sqrt{2}}{2}a_{\mathrm{MgO}}\Big)\Big)^2+\Big((l'+1/2)\Big(\frac{\sqrt{2}}{2}a_{\mathrm{Pd}}\Big)\Big)^2+\Big(\sqrt{2}m\Big(\frac{\sqrt{2}}{2}a_{\mathrm{MgO}}\Big)\Big)^2\\
&+\Big((n+1/2)\Big(\frac{\sqrt{2}}{2}a_{\mathrm{MgO}}\Big)\Big)^2\Bigg]^{1/2}\Bigg)\\
&+\Phi_{\mathrm{Pd-O}}\Bigg(\Bigg[\Bigg(d+(l+1/2)\Big(\frac{\sqrt{2}}{2}a_{\mathrm{MgO}}\Big)\Big)^2+\Big((l'+1/2)\Big(\frac{\sqrt{2}}{2}a_{\mathrm{Pd}}\Big)\Big)^2+\Big(\sqrt{2}(m+1/2)\Big(\frac{\sqrt{2}}{2}a_{\mathrm{MgO}}\Big)\Big)^2\\
&+\Big(n\Big(\frac{\sqrt{2}}{2}a_{\mathrm{MgO}}\Big)\Big)^2\Bigg]^{1/2}\Bigg)\\
&+\Phi_{\mathrm{Pd-O}}\Bigg(\Bigg[\Bigg(d+l\Big(\frac{\sqrt{2}}{2}a_{\mathrm{MgO}}\Big)+(l'+1/2)\Big(\frac{\sqrt{2}}{2}a_{\mathrm{Pd}}\Big)\Big)^2+\Big(\sqrt{2}(m+1/2)\Big(\frac{\sqrt{2}}{2}a_{\mathrm{MgO}}\Big)\Big)^2\\
&+\Big(n\Big(\frac{\sqrt{2}}{2}a_{\mathrm{MgO}}\Big)\Big)^2\Bigg]^{1/2}\Bigg)\\
&+\Phi_{\mathrm{Pd-O}}\Bigg(\Bigg[\Bigg(d+(l+1/2)\Big(\frac{\sqrt{2}}{2}a_{\mathrm{MgO}}\Big)\Big)^2+\Big((l'+1/2)\Big(\frac{\sqrt{2}}{2}a_{\mathrm{Pd}}\Big)\Big)^2+\Big(\sqrt{2}m\Big(\frac{\sqrt{2}}{2}a_{\mathrm{MgO}}\Big)\Big)^2\\
&+\Big((n+1/2)\Big(\frac{\sqrt{2}}{2}a_{\mathrm{MgO}}\Big)\Big)^2\Bigg]^{1/2}\Bigg)\Bigg\} \qquad (2)
\end{aligned}
$$

where l, l', m, and n are atomic indices perpendicular to or parallel with the interface plane. Equation (2) is the specific form of equation (1) for the fcc-M/MgO(110) interface. We want to solve it to get $\Phi_{\mathrm{Pd-Mg}}$ and $\Phi_{\mathrm{Pd-O}}$. This is quite a complex inverse problem, and some skills are desired.

First, by introducing two variables

$$E_{\pm}=E_{\mathrm{Pd}\to\mathrm{Mg}}\pm E_{\mathrm{Pd}\to\mathrm{O}} \qquad \Phi_{\pm}=\Phi_{\mathrm{Pd-Mg}}\pm\Phi_{\mathrm{Pd-O}} \qquad (3)$$

equation (2) is changed to

$$
\begin{aligned}
E_{\pm}(d)=&\sum_{l,l'=0}^{\infty}\sum_{m,n=-\infty}^{\infty}(\pm1)^{l+l'+m+n}\\
&\times\Phi_{\pm}\Bigg(\Bigg[\Bigg(d+\frac{1}{2}l\Big(\frac{\sqrt{2}}{2}a_{\mathrm{MgO}}\Big)+\frac{1}{2}l'\Big(\frac{\sqrt{2}}{2}a_{\mathrm{Pd}}\Big)\Big)^2\\
&+((\sqrt{2}m)^2+n^2)\Big(\frac{\sqrt{2}}{4}a_{\mathrm{MgO}}\Big)^2\Bigg]^{1/2}\Bigg). \qquad (4)
\end{aligned}
$$

Then, by defining a medium variable $H_{\pm}$

$$
\begin{aligned}
H_{\pm}(d)=&\sum_{m,n=-\infty}^{\infty}(\pm1)^{m+n}\\
&\times\Phi_{\pm}\Bigg(\sqrt{d^2+(2m^2+n^2)\Big(\frac{\sqrt{2}}{4}a_{\mathrm{MgO}}\Big)^2}\Bigg), \qquad (5)
\end{aligned}
$$

equation (4) can be simplified to

$$
\begin{aligned}
E_{\pm}(d)=&\sum_{l,l'=0}^{\infty}(\pm1)^{l+l'}H_{\pm}\Bigg(d+\frac{1}{2}l\Big(\frac{\sqrt{2}}{2}a_{\mathrm{MgO}}\Big)\\
&+\frac{1}{2}l'\Big(\frac{\sqrt{2}}{2}a_{\mathrm{Pd}}\Big)\Bigg). \qquad (6)
\end{aligned}
$$

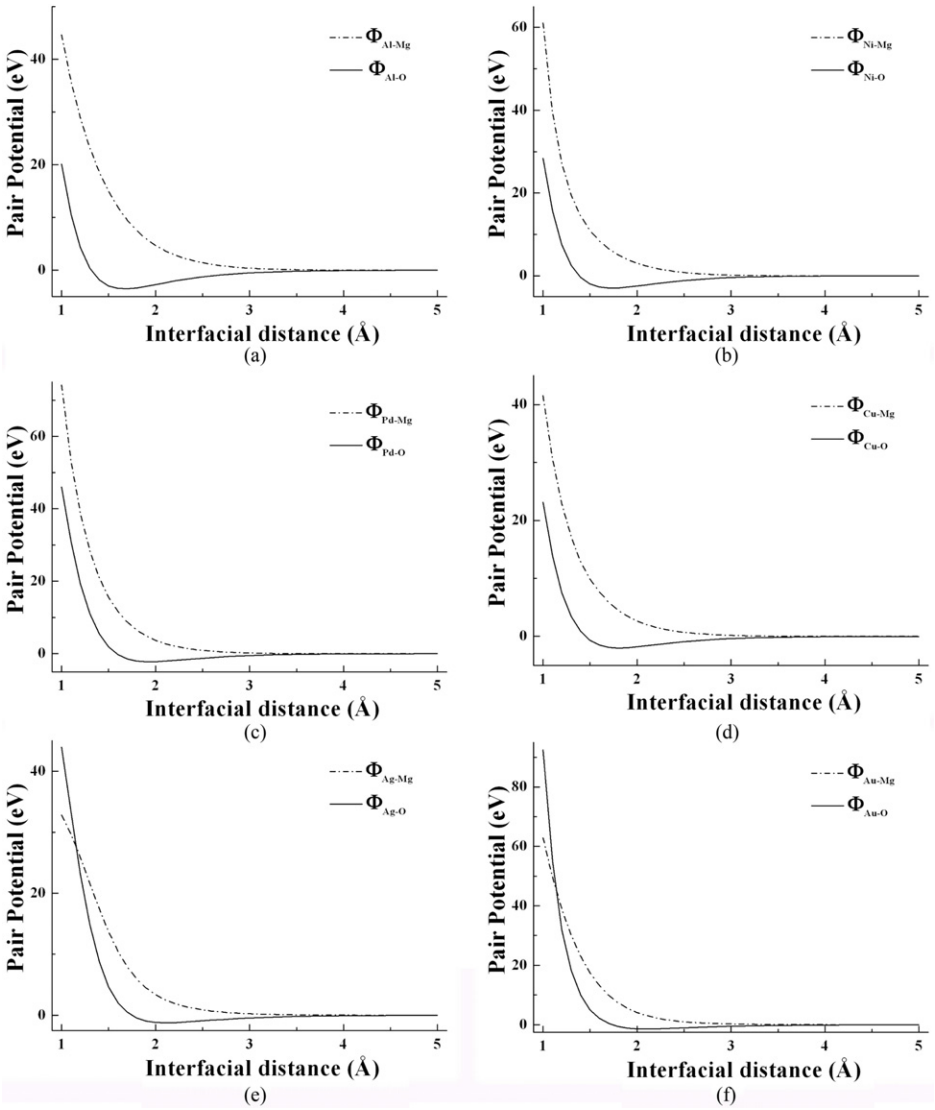

Figure 3. Potential curves of $\Phi_{\mathrm{M-Mg}}(d)$ and $\Phi_{\mathrm{M-O}}(d)$.

Now, we use the vectors:

$$E = \begin{pmatrix} E_+ \\ E_- \end{pmatrix} \qquad H = \begin{pmatrix} H_+ \\ H_- \end{pmatrix} \qquad \Phi = \begin{pmatrix} \Phi_+ \\ \Phi_- \end{pmatrix} \tag{7}$$

to rewrite equation (6) in the following form

$$E(d) = \sum_{l,l'=0}^{\infty} A_{l,l'} H\left(d + \frac{1}{2}l\left(\frac{\sqrt{2}}{2}a_{\mathrm{MgO}}\right) + \frac{1}{2}l'\left(\frac{\sqrt{2}}{2}a_{\mathrm{Pd}}\right)\right) \tag{8}$$

$$A_{l,l'} = C_l M_{l'} \tag{9}$$

where $A_{l,l'}$, C_l, and $M_{l'}$ are all 2×2 matrices.

It is very interesting to find that equation (8) can be solved by using the inversion coefficients $\{B_{L,L'}\}$, which are calculated by the formula:

$$B_{L,L'} = D_L N_{L'} \qquad \sum_{L=0}^{\infty}\sum_{l=0}^{L} D_{L-l}C_l = \delta_{L,0}$$

$$\sum_{L'=0}^{\infty}\sum_{l'=0}^{L'} N_{L'-l'}M_{l'} = \delta_{L',0} \qquad \forall L, L', l, l' \in \overline{\mathbf{Z}^-}. \tag{10}$$

From equations (8) to (10), it is easy to prove that

$$\begin{aligned}
&\sum_{i,j=0}^{\infty} D_i N_j E\left(d + i\frac{\sqrt{2}}{4}a_{\mathrm{MgO}} + j\frac{\sqrt{2}}{4}a_{\mathrm{Pd}}\right) \\
&= \sum_{i,j=0}^{\infty} D_i N_j \sum_{l,l'=0}^{\infty} C_l M_{l'} H\left(d + \frac{1}{2}(l+i)\left(\frac{\sqrt{2}}{2}a_{\mathrm{MgO}}\right)\right. \\
&\quad \left. + \frac{1}{2}(l'+j)\left(\frac{\sqrt{2}}{2}a_{\mathrm{Pd}}\right)\right) \\
&= \sum_{i=0}^{\infty} D_i \sum_{l=0}^{\infty} C_l \sum_{j=0}^{\infty} N_j \sum_{l'=0}^{\infty} M_{l'} \\
&\quad \times H\left(d + \frac{1}{2}(l+i)\left(\frac{\sqrt{2}}{2}a_{\mathrm{MgO}}\right)\right. \\
&\quad \left. + \frac{1}{2}(l'+j)\left(\frac{\sqrt{2}}{2}a_{\mathrm{Pd}}\right)\right) \\
&= \sum_{L=0}^{\infty}\sum_{l=0}^{L} D_{L-l}C_l \sum_{L'=0}^{\infty}\sum_{l'=0}^{L'} N_{L'-l'}M_{l'}
\end{aligned}$$

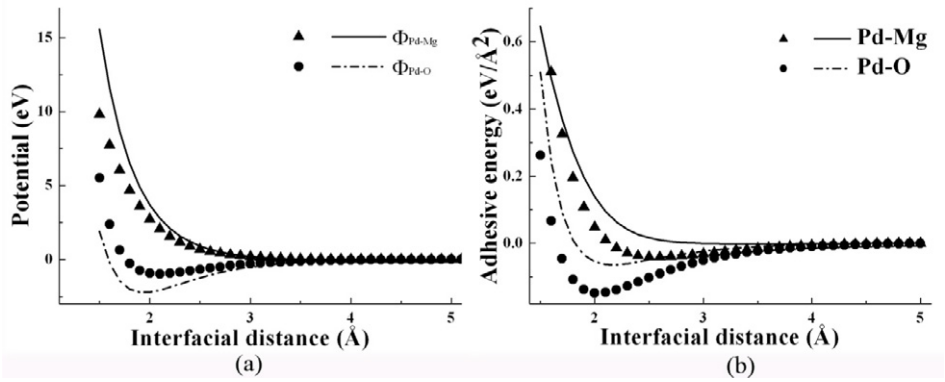

Figure 4. (a) Potential curves of $\Phi_{\mathrm{Pd-Mg}}(d)$ and $\Phi_{\mathrm{Pd-O}}(d)$, where triangles and circles are potentials of Pd/MgO(001), and solid curves are potentials of Pd/MgO(110). (b) Adhesive energy versus d curves of Pd/MgO(110) interfaces. Triangles and circles are original *ab initio* data, and solid curves are recalculated data by interfacial potentials of Pd/MgO(001).

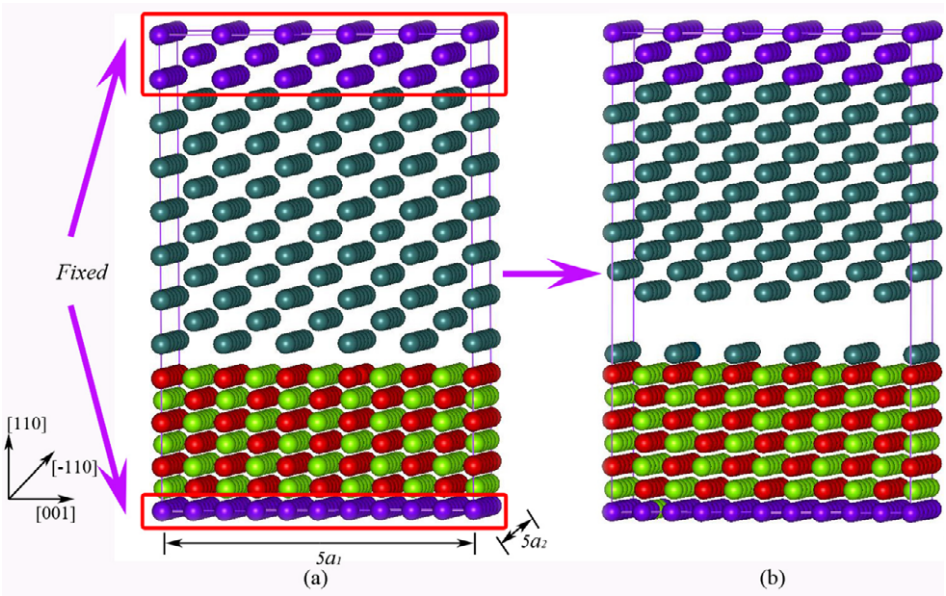

Figure 5. (a) Initial interface structure of Pd/MgO(110). (b) Broken interface structure of Pd/MgO(110). The interface area is $5a_1 \times 5a_2$, where a_1 is the lattice constant of MgO and a_2 is equal to $\sqrt{2}/2a_1$.

$$\times H\left(d+\frac{1}{2}L\left(\frac{\sqrt{2}}{2}a_{\mathrm{MgO}}\right)+\frac{1}{2}L'\left(\frac{\sqrt{2}}{2}a_{\mathrm{Pd}}\right)\right)$$
$$=\sum_{L=0}^{\infty}\sum_{l=0}^{L}\delta_{L,0}\delta_{L',0}H\left(d+\frac{1}{2}L\left(\frac{\sqrt{2}}{2}a_{\mathrm{MgO}}\right)+\frac{1}{2}L'\left(\frac{\sqrt{2}}{2}a_{\mathrm{Pd}}\right)\right)$$
$$=H(d). \tag{11}$$

So $H(d)$ is

$$H(d)=\sum_{i,j=0}^{\infty}D_iN_jE\left(d+i\frac{\sqrt{2}}{4}a_{\mathrm{MgO}}+j\frac{\sqrt{2}}{4}a_{\mathrm{Pd}}\right). \tag{12}$$

Half of the inverse problem of equation (2) has been solved. The remaining work is to solve equation (5). For this purpose, it is rewritten as

$$H(d)=\sum_{k=0}^{\infty}(\pm1)^kh(k)\Phi\left(\sqrt{d^2+k(\sqrt{2}a_{\mathrm{MgO}}/4)^2}\right). \tag{13}$$

It can be proved that $h(k)$ is equal to the number of integer solutions for $k=2m^2+n^2$ and more details can be seen in [13]. Again, another inversion coefficient $g(n)$ is introduced, which satisfies the recursive relation:

$$\sum_{m=0}^{\infty}h(m)g(k-m)=\delta_{k,0}. \tag{14}$$

From equations (13) and (14), it is not difficult to prove that:

$$\sum_{n=0}^{\infty}(\pm1)^ng(n)H_{\pm}\left(\sqrt{d^2+n\left(\frac{\sqrt{2}}{4}a_{\mathrm{MgO}}\right)^2}\right)$$
$$=\sum_{n=0}^{\infty}(\pm1)^ng(n)\sum_{m=0}^{\infty}(\pm1)^mh(m)$$
$$\times\Phi_{\pm}\left(\sqrt{d^2+n\left(\frac{\sqrt{2}}{4}a_{\mathrm{MgO}}\right)^2+m\left(\frac{\sqrt{2}}{4}a_{\mathrm{MgO}}\right)^2}\right)$$
$$=\sum_{k=0}^{\infty}(\pm1)^k\sum_{m=0}^{k}h(m)g(k-m)$$

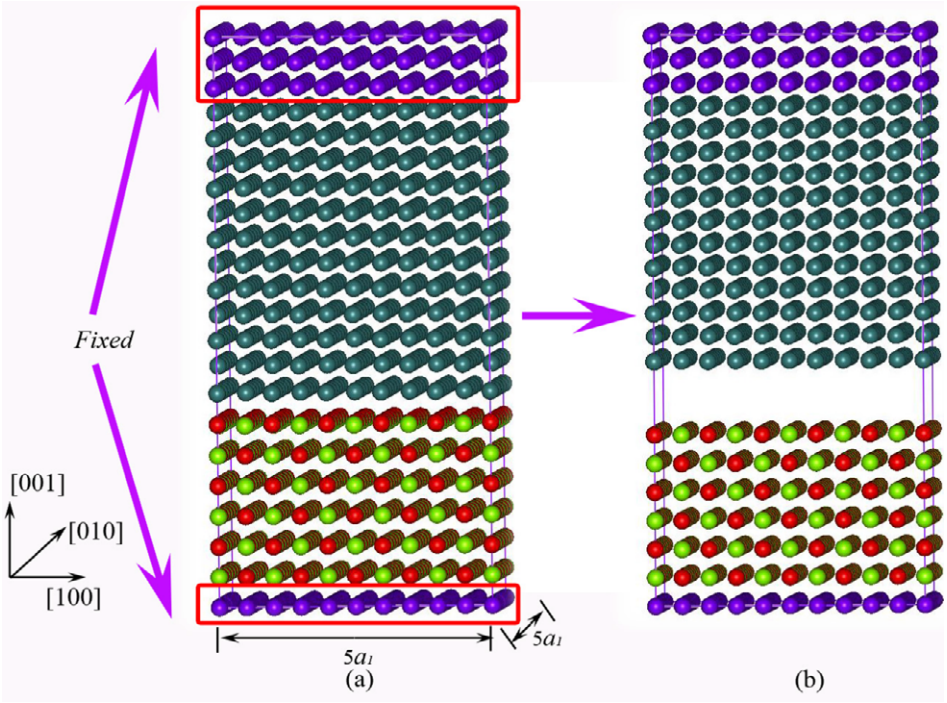

Figure 6. (a) Initial interface structure of Pd/MgO(001). (b) Broken interface structure of Pd/MgO(001). The interface area is $5a_1 \times 5a_1$. This result is consistent with our previous study in [14].

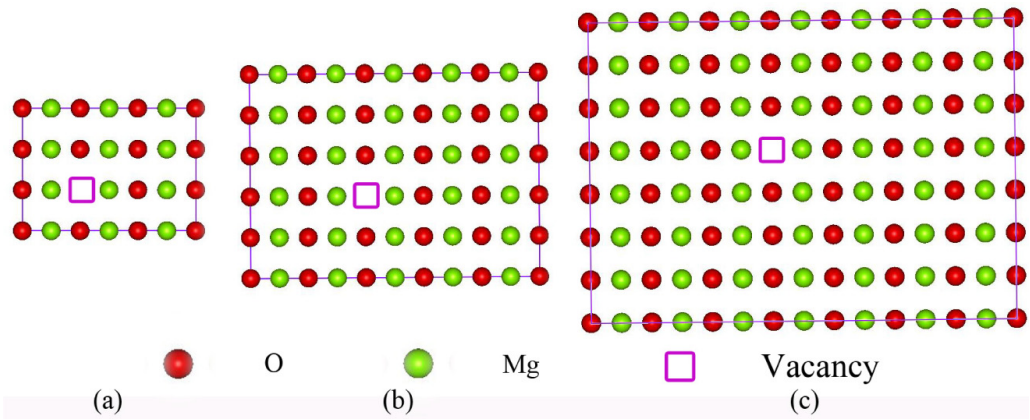

Figure 7. Interface structure of Pd/MgO(110) including an oxygen vacancy. The interface area is (a) $3a_1 \times 3a_2$, (b) $5a_1 \times 5a_2$, and (c) $10a_1 \times 10a_2$.

$$\times \Phi_{\pm}\left(\sqrt{d^2 + k\left(\frac{\sqrt{2}}{4}a_{\mathrm{MgO}}\right)^2}\right)$$
$$= \sum_{k=0}^{\infty}(\pm 1)^k \delta_{k,0}\Phi_{\pm}\left(\sqrt{d^2 + k\left(\frac{\sqrt{2}}{4}a_{\mathrm{MgO}}\right)^2}\right)$$
$$= \Phi_{\pm}(d). \tag{15}$$

In other words, equation (5)'s solution is

$$\Phi_{\pm}(d) = \sum_{n=0}^{\infty}(\pm 1)^n g(n) H_{\pm}\left(\sqrt{d^2 + n\left(\frac{\sqrt{2}}{4}a_{\mathrm{MgO}}\right)^2}\right). \tag{16}$$

The corresponding coefficients $h(k)$ and $g(k)$ are listed in table 2, while the coefficients $A_{l,l'}$ and $B_{l,l'}$ are shown in table 3.

Summarizing equations (12) and (16), we achieve the final inversion formula of equation (2)

$$\begin{pmatrix}\Phi_+(d)\\ \Phi_-(d)\end{pmatrix} = \sum_{n=0}^{\infty}(\pm 1)^n g(n) \sum_{i,j=0}^{\infty} B_{i,j}$$
$$\times \begin{pmatrix} E_+\left(\sqrt{d^2 + n\left(\frac{\sqrt{2}}{4}a_{\mathrm{MgO}}\right)^2} + i\frac{\sqrt{2}}{4}a_{\mathrm{MgO}} + j\frac{\sqrt{2}}{4}a_{\mathrm{Pd}}\right) \\ E_-\left(\sqrt{d^2 + n\left(\frac{\sqrt{2}}{4}a_{\mathrm{MgO}}\right)^2} + i\frac{\sqrt{2}}{4}a_{\mathrm{MgO}} + j\frac{\sqrt{2}}{4}a_{\mathrm{Pd}}\right)\end{pmatrix} \tag{17}$$

where $E_{\pm}$, a_{MgO}, and a_{Pd} all come from previous DFT calculations. So the interfacial potentials $\Phi_{\mathrm{Pd-Mg}}(d)$ and

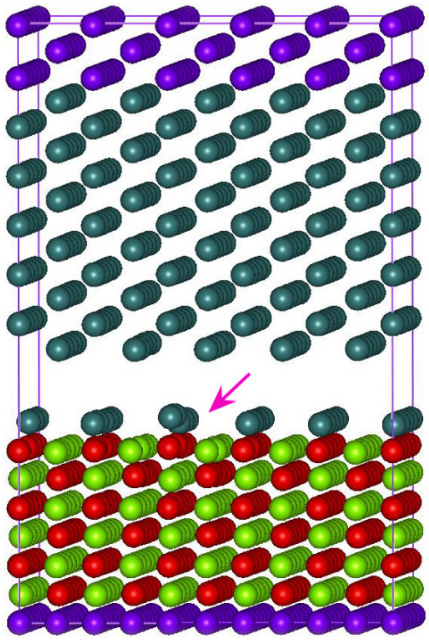

Figure 8. Broken interface structure of Pd/MgO(110) including an oxygen vacancy (marked by the arrow).

Table 2. Values of original coefficients $h(k)$ and inversion coefficients $g(k)$.

k	$h(k)$	$g(k)$
0	1	1
1	2	−2
2	2	2
3	4	−4
4	2	10
5	0	−16
6	4	20
7	0	−32
8	2	58

$\Phi_{\mathrm{Pd-O}}(d)$ are

$$\Phi_{\mathrm{Pd-Mg}}(d) = \frac{\Phi_+(d) + \Phi_-(d)}{2}$$
$$\Phi_{\mathrm{Pd-O}}(d) = \frac{\Phi_+(d) - \Phi_-(d)}{2}. \tag{18}$$

2.4. The inverted pair potentials

Based on the method introduced above, the interfacial potential curves $\Phi_{\mathrm{Pd-}Mg}$ and $\Phi_{\mathrm{Pd-O}}$ are obtained, as shown in figure 3. For applications, they are fitted by the Rahman–Stillinger–Lemberg (RSL2) potential function:

$$\Phi = D_0 \mathrm{e}^{y(1-\frac{R}{R_0})} + \frac{a_1}{1+\mathrm{e}^{b_1(R-c_1)}} + \frac{a_2}{1+\mathrm{e}^{b_2(R-c_2)}} + \frac{a_3}{1+\mathrm{e}^{b_3(R-c_3)}}. \tag{19}$$

The potential parameters are listed in table 4, including the results for many other fcc-M/MgO(110) interfaces in the same way. In addition, the parameters of Pd/MgO(001) are also listed in table 4. By the way, figure 2 demonstrates the recalculated interfacial adhesive energies by potentials, which agree quite well with the original *ab initio* data. This check shows that our inverse method is self-consistent.

Table 3. Values of original coefficients $A_{l,l'}$ and inversion coefficients $B_{l,l'}$.

l	l'	$A(l,l')$	$B(l,l')$
0	0	$\begin{bmatrix}1&0\\0&1\end{bmatrix}$	$\begin{bmatrix}1&0\\0&1\end{bmatrix}$
1	0	$\begin{bmatrix}1&0\\0&-1\end{bmatrix}$	$\begin{bmatrix}-1&0\\0&1\end{bmatrix}$
0	1	$\begin{bmatrix}1&0\\0&-1\end{bmatrix}$	$\begin{bmatrix}-1&0\\0&1\end{bmatrix}$
1	1	$\begin{bmatrix}1&0\\0&1\end{bmatrix}$	$\begin{bmatrix}1&0\\0&1\end{bmatrix}$
2	0	$\begin{bmatrix}1&0\\0&1\end{bmatrix}$	$\begin{bmatrix}0&0\\0&0\end{bmatrix}$
2	1	$\begin{bmatrix}1&0\\0&-1\end{bmatrix}$	$\begin{bmatrix}0&0\\0&0\end{bmatrix}$
2	2	$\begin{bmatrix}1&0\\0&1\end{bmatrix}$	$\begin{bmatrix}0&0\\0&0\end{bmatrix}$
1	2	$\begin{bmatrix}1&0\\0&-1\end{bmatrix}$	$\begin{bmatrix}0&0\\0&0\end{bmatrix}$
0	2	$\begin{bmatrix}1&0\\0&1\end{bmatrix}$	$\begin{bmatrix}0&0\\0&0\end{bmatrix}$

3. The fracture of the Pd/MgO(110) interface

In our previous work [14], we have pointed out that the Pd/MgO(001) interface tends to break between the MgO and Pd interface (see figure 6). But the pair potentials obtained for the Pd/MgO(001) interface do not work well with the Pd/MgO(110) interface. To illustrate this point, a simple comparison is displayed in figure 4. We can see that both potential and adhesive energy calculated by the potentials of Pd/MgO(001) do not match well with those of Pd/MgO(110). So it is necessary to study the Pd/MgO(110) interface by Pd/MgO(110) interfacial potentials.

Now we intend to learn how the fracture of the Pd/MgO(110) interface occurs by using the Pd/MgO(110) potentials. The atomistic simulation method used in this work is energy minimization performed by Cerius[2] software. In addition, the interatomic pair potentials employed in Pd and MgO slabs, such as $\Phi_{\mathrm{Pd-Pd}}$, $\Phi_{\mathrm{Mg-Mg}}$, $\Phi_{\mathrm{Mg-O}}$, and $\Phi_{\mathrm{O-O}}$, follow our previous works [12].

As revealed by *ab initio* calculations, the equilibrium structure of the Pd/MgO interface is Pd on top of O ions, as illustrated in figure 5(a). The interface model consists of 15 Pd monolayers (MLs) and seven MgO MLs with an interface area of $5a_1 \times 5a_2$. Moreover, as the boundary condition, the last three Pd MLs and one MgO ML are fixed in atomistic simulation (see figure 5). During the simulation, we let the fixed Pd layers be pulled away from MgO slab step by step. At each step, the free atoms and ions are fully relaxed. The variations of total energy and tensile stress in this process are displayed in figure 9(a).

As a result, we find that the fracture of Pd/MgO(110) occurs between the first and second Pd MLs (see figure 5(b)), different from the Pd/MgO(001) case (see figure 6(b)). In figure 6(b), the fracture of Pd/MgO(001) is believed to occur between Pd and MgO. This can be attributed to their different adhesive properties on the interface. For a brief discussion,

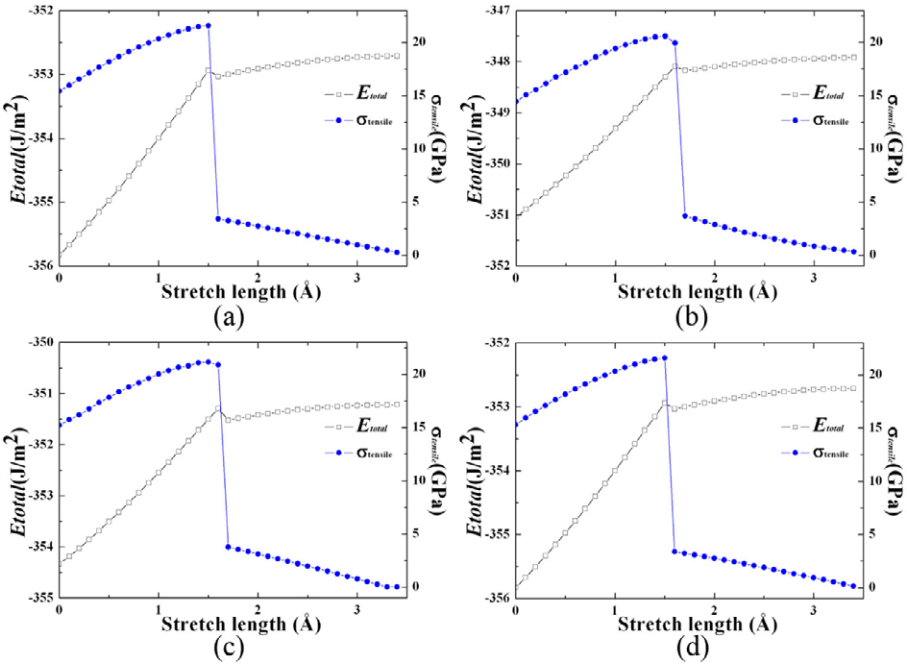

Figure 9. Curves of total energy and tensile stress versus stretch length. (a) $\sigma_v = 0$, (b) $\sigma_v = 1/9$, (c) $\sigma_v = 1/25$, and (d) $\sigma_v = 1/49$.

Table 4. Potential parameters of M/MgO(110) and Pd/MgO(001).

	D_0 (eV)	R_0 (Å)	Y	a_1 (eV)	b_1 (Å^{-1})	c_1 (Å)	a_2 (eV)	b_2 (Å^{-1})	c_2 (Å)	a_3 (eV)	b_3 (Å^{-1})	c_3 (Å)
M/MgO(110)												
Φ_{Al-Mg}	2.45	1.00	7.42	740.17	2.03	0.20	−518.95	1.85	0.08	0.70	1.74	2.50
Φ_{Al-O}	0.01	1.00	5.43	0.38	1.39	2.13	−26.53	1.81	0.93	196.28	4.66	0.65
Φ_{Ni-Mg}	35.78	1.00	6.91	467.07	2.59	0.45	−546.87	2.65	0.24	−0.09	2.59	3.74
Φ_{Ni-O}	465.41	1.00	1.73	−0.92	3.07	2.43	−2840.83	1.70	0.25	421.19	1.66	0.84
Φ_{Pd-Mg}	32.26	1.00	4.98	740.14	2.31	0.40	−518.97	2.17	0.37	0.35	2.68	2.63
Φ_{Pd-O}	0.01	1.00	5.44	1.39	3.33	1.83	−26.09	2.07	1.15	196.29	4.33	0.81
Φ_{Cu-Mg}	18.31	1.00	4.38	186.89	2.13	0.35	−41.11	1.88	0.65	−0.42	34.44	1.51
Φ_{Cu-O}	218.64	1.00	1.82	161.33	3.71	0.56	−2086.21	1.81	0.08	368.41	1.80	0.54
Φ_{Ag-Mg}	5.01	1.00	1.93	4.06	2.62	2.03	−87.31	2.64	0.83	88.01	3.63	1.18
Φ_{Ag-O}	1.44	1.00	2.71	5.13	3.51	1.55	−94.59	1.75	0.0	92.62	5.24	1.04
Φ_{Au-Mg}	0.38	1.00	5.51	9.17	8.53	0.62	−82.35	2.00	1.22	542.66	2.00	0.33
Φ_{Au-O}	39.13	1.00	4.18	143.76	1.99	0.28	−42.62	1.85	1.08	365.91	6.66	0.71
Pd/MgO(001)												
Φ_{Pd-Mg}	32.81	1.00	3.64	102.55	3.49	0.84	−85.93	2.75	0.47	49.71	1.51	0.01
Φ_{Pd-O}	5.88	1.00	2.53	27.15	2.64	0.65	−37.87	1.55	0.48	201.55	5.70	0.87

ab initio calculations reveal that the adhesive energy on the ideal interface is about 0.15 eV Å^{-2} for Pd/MgO(110) and 0.10 eV Å^{-2} for Pd/MgO(001). This suggests that the bonding of Pd/MgO(110) is stronger than that of Pd/MgO(001) on the interface. So it is understandable that the fracture processes are quite different for these two orientations.

Furthermore, we consider the oxygen vacancy on the MgO surface and define the vacancy density $\sigma_v = N/S$, where N and S denote the number of vacancies and the unit cell on the surface, respectively. For example, there is one oxygen vacancy on the surface, as shown in figure 7(b), and the interface area is $5a_1 \times 5a_2$, so the value of σ_v is 1/25. In this work, we choose the σ_vs values to be 1/9, 1/25, 1/49, and 0. The zero represents the ideal interface and the interface area for this case is $5a_1 \times 5a_2$. The calculation reveals that the fracture always occurs between the first and second Pd MLs, just the same as in the no vacancy case. An example of $\sigma_v = 1/25$ is displayed in figure 8. In addition, the total energy and tensile stress (σ_{stress}) variations are presented in figure 9. Although the curves of σ_{stress} are similar for different σ_v, the ideal case seems to have a greater value at the same stretch length. So the fracture is the most difficult to occur in this case. Moreover, we also find that the value of σ_{stress} increases with the decrease of σ_v. In particular, the curve of $\sigma_v = 1/49$ has almost the same σ_{stress} as the ideal case. For instance, when the interface breaks, the value of σ_{stress} is 19.9 GPa, 20.9 GPa, 21.6 GPa, and 21.6 GPa for the case of $\sigma_v = 1/9$, 1/25, 1/49, and 0, respectively. Therefore, we suppose that the vacancy existing

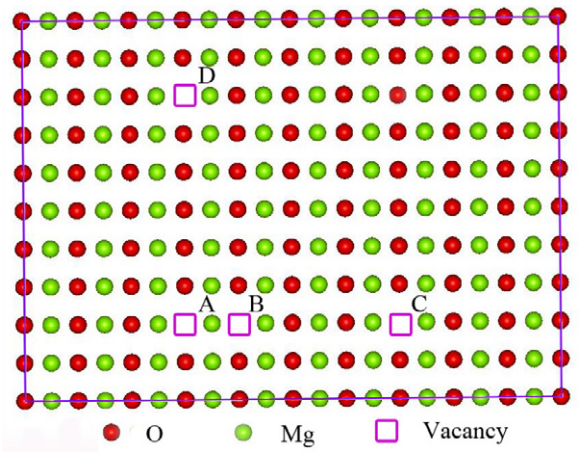

Figure 10. Surface structure of MgO(110) including two oxygen vacancies. The interface area is $10a_1 \times 10a_2$.

on the surface is in favor of the occurrence of fracture and the fracture occurs more easily at a high vacancy density interface.

On the other hand, we want to know how the fracture occurs, when oxygen vacancies are set at different positions. Therefore, we assume there are two oxygen vacancies existing at AB, AC, and AD respectively (see figure 10). The total energy and tensile stress variations in all situations are calculated and have been presented in figure 11. From our calculations, we find that they all break between the first and second Pd MLs, just like the former cases. But it seems that the fracture occurs more easily in the AB case, because the σ_{stress} of AB is smaller than the other cases. For example, as the interface breaks, the value of σ_{stress} is 19.4 GPa, 21.1 GPa, and 21.2 GPa for the case of AB, AC, and AD respectively. Why is there such a big difference between AB and the other cases? To answer this question, a comparison of their broken MgO(110) surface is displayed in figure 12. Two separate vacancies can be seen clearly in the AC and AD cases, but in the AB case they are combined together. That is to say, if two oxygen vacancies on the MgO(110) surface are placed far enough apart, although their relative positions can be different, we will always get two similar vacancy structures. On the contrary, when two vacancies are set very close, such as in the AB case, they tend to combine together and form a new vacancy structure. Based on the above discussions, we can see that oxygen vacancies placed at different positions might bring different vacancy structures, and thus will affect the fracture on the interface.

4. Conclusion

In this work, we use the Chen–Möbius method to calculate the interatomic potentials across fcc-M/MgO(110) interfaces. The potentials are analytically derived based on the pair interaction assumption, and then numerically calculated.

For an application, we use the resultant potentials to study the fracture processes of Pd/MgO(001) and Pd/MgO(110) interfaces. This shows that the fracture occurs between the first and second Pd ML for the Pd/MgO(110) interface, and right on the interface for the Pd/MgO(001) interface. This difference may come from their different adhesive energies at the interface. Furthermore, we also take into account the effect of the oxygen vacancies on the fracture of the Pd/MgO(110) interface. Our studies reveal that the presence of an oxygen vacancy favors the occurrence of fracture and higher vacancy density makes the interface easier to break. In addition, we also find that oxygen vacancies existing on the MgO(110) surface tend to form separate vacancy structures while the distance

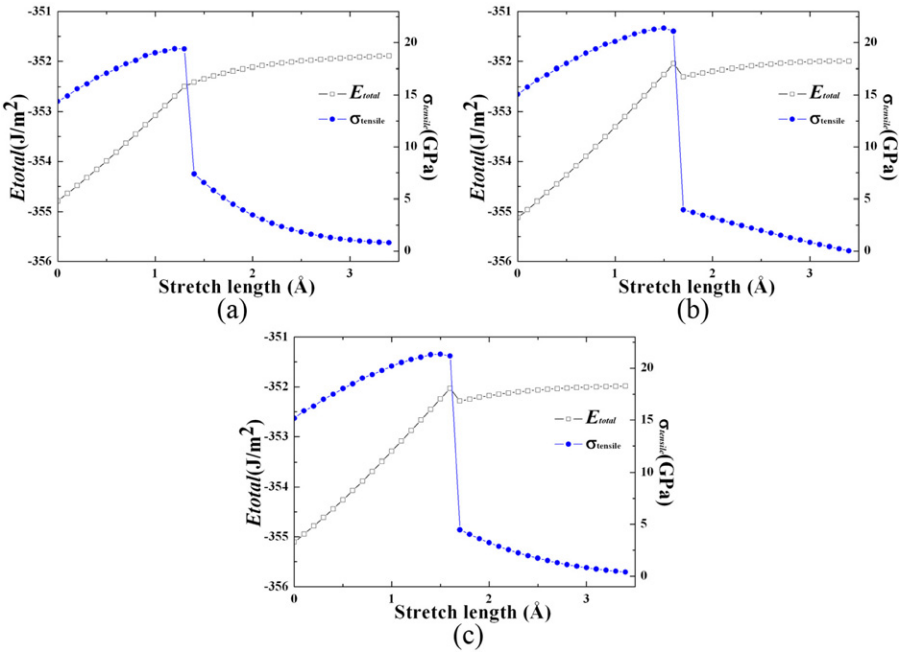

Figure 11. Curves of total energy and tensile stress versus stretch length. Two oxygen vacancies are set at (a) A and B, (b) A and C, and (c) A and D.

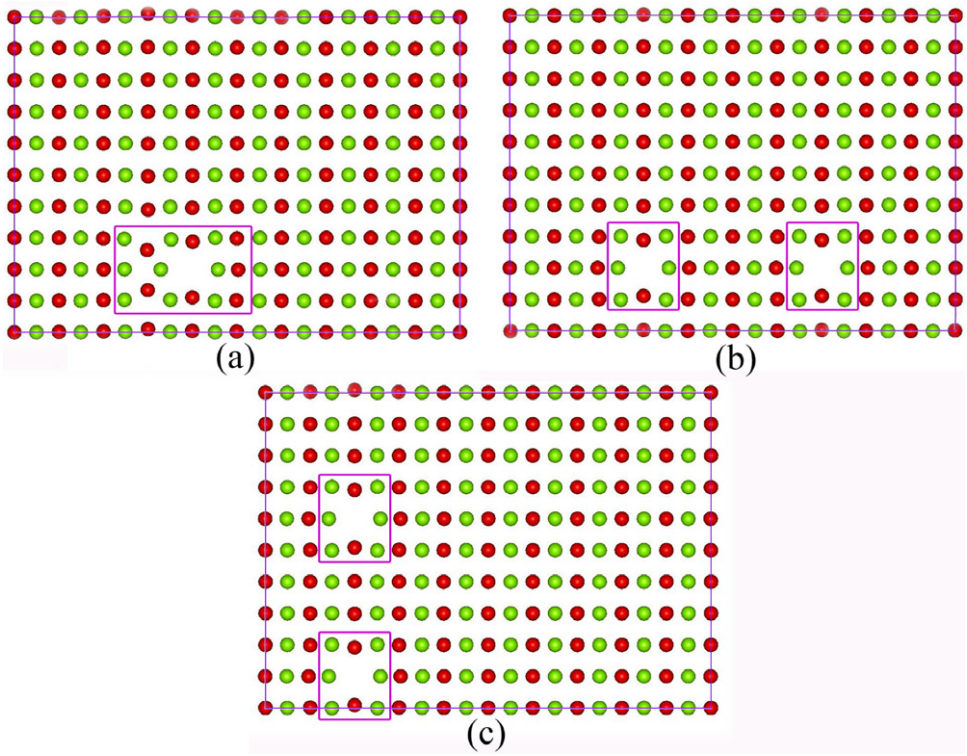

Figure 12. Broken surface structure of MgO(110) including two oxygen vacancies. Two oxygen vacancies are set at (a) A and B, (b) A and C, and (c) A and D.

between them is large enough, but if they are close enough to each other, they prefer to form a larger vacancy structure, which conversely accelerates the occurrence of fracture. Based on the above discussions, we believe the interatomic potential obtained in this paper is a powerful tool to study interface structures and related mechanical properties.

Acknowledgments

This work is supported by the Nature Science Foundation of China (NSFC, No. 50531050) and 973 project (No. 2006CB605100). We would like to acknowledge helpful discussions with Dr Long Yao.

References

[1] Ernst F 1995 Metal–oxide interfaces *Mater. Sci. Eng.* R **14** 97
[2] Sinnott S B and Dickey E C 2003 Ceramic/metal interface structures and their relationship to atom- and meso-scale properties *Mater. Sci. Eng.* R **43** 1
[3] Rühle M 1996 Structure and composition of metal/ceramic interfaces *J. Eur. Ceram. Soc.* **16** 353
[4] Guénard P, Renaud G and Villette B 1996 Structure, translational state and morphology of the Ag/MgO(001) interface during its formation *Physica* B **221** 205
[5] Giordano L, Baistrocchi M and Pacchioni G 2005 Bonding of Pd, Ag, and Au atoms on MgO(100) surfaces and MgO/Mo(100) ultra-thin films: a comparative DFT study *Phys. Rev.* B **72** 115403
[6] Purton J A *et al* 1999 Comparison of atomistic simulations and pseudopotential calculations of the MgO{100}/Ag{100} and MgO{110}/Ag{110} interfaces *J. Chem. Phys.* **110** 8090
[7] Altieri S, Contri S F and Valeri S 2007 Hydrolysis at MgO(100)/Ag(100) oxide–metal interfaces studied by O 1s x-ray photoelectron and $MgKL_{23}L_{23}$ Auger spectroscopy *Phys. Rev.* B **76** 205413
[8] Pascual J L, Savoini B and González R 2007 Electronic adsorption spectra of Cu^{2+} in MgO: *ab initio* theory and experiment *Phys. Rev.* B **70** 045109
[9] Duffy D M, Harding J H and Stoneham A M 1992 Atomistic modeling of the metal–oxide interface with image interactions *Acta Metall. Mater.* **40** S11
[10] Purton J A, Parker C and Bullett D W 1997 Computer modeling of metal–oxide interfaces *J. Phys.: Condens. Matter* **9** 5709
[11] Chen N X 1990 Modified Möbius inverse formula and its applications in physics *Phys. Rev. Lett.* **64** 1193
[12] Long Y, Chen N X and Zhang W Q 2005 Pair potentials for a metal–ceramic interface by inversion of adhesive energy *J. Phys.: Condens. Matter* **17** 2045
[13] Long Y, Chen N X and Wang H Y 2005 Theoretical investigations of misfit dislocations in Pd/MgO(001) interfaces *J. Phys.: Condens. Matter* **17** 6149
[14] Long Y and Chen N X 2008 Theoretical study of misfit dislocation in interface dynamics *Comput. Mater. Sci.* **44** 721
[15] Kresse G and Furthmüller J 1996 Efficient iterative schemes for *ab initio* total-energy calculations using a plane-wave basis set *Phys. Rev.* B **54** 11169
[16] Vanderbilt D 1990 Soft self-consistent pseudopotentials in a generalized eigenvalue formalism *Phys. Rev.* B **41** 7892
[17] Hohenberg P and Kohn W 1964 Inhomogeneous electron gas *Phys. Rev.* **136** B864